Piezoelectric Energy Harvesting Characteristics of Barium Titanate Based Composite Laminates under Cyclic Concentrated Loads

Fumio Narita[*], Xiaolong Zhu and Yasuhide Shindo

Department of Materials Processing, Graduate School of Engineering, Tohoku University, Aoba-yama 6-6-02, Sendai 980-8579, Japan

Abstract: We investigate the dynamic electromechanical behavior in barium titanate (BT) based composite cantilevers under cyclic concentrated loads in a combined numerical and experimental approach. The laminated composite cantilever consists of the BT and copper (Cu) layers, and the BT layer has sensing and driving electrodes. The output voltage of the cantilevers due to cyclic bending were calculated by three dimensional finite element method. The output voltage was then measured, and numerical simulations were compared with test results to verify the finite element model. The influences of sensing electrode geometry and load resistance on the dynamic electromechanical fields were examined in detail.

Keywords: Piezomechanics, testing and simulation, barium titanate/copper laminate, bending, energy harvesting.

1. INTRODUCTION

Piezoelectric ceramic composites have become very popular in sensing and actuation. They also appear to be good candidates for applications, such as energy harvesters [1-2]. Vatansever *et al*. [3] discussed the voltage output of various piezoelectric materials subjected to the impact of water drops. Wong *et al*. [4] also examined the dynamic characteristics of piezoelectric beam under water droplet impact. Okayasu and Watanabe [5] studied the power generated in lead zirconate titanate (PZT) piezoelectric ceramics under various cyclic loading conditions. In addition, some researchers have focused on the design of self-powering, self-sensing and self-controlling devices [6]. Recently, Narita and Shindo [7] studied numerically and experimentally the bending behavior and sensor property of BT piezoelectric unimorph cantilevers subjected to alternating current (AC) electric fields.

BT is one of the most studied lead-free materials because of its extraordinary ferroelectric properties [8, 9]. This paper deals with the dynamic electro-mechanical behavior of BT piezoelectric composite energy harvesters with sensing and driving electrodes subjected to cyclic concentrated loads. A three dimensional finite element analysis (FEA) was carried out to obtain the output voltage in the BT harvesters, and the effect of sensing electrode geometry on the output voltage was predicted. The output voltage was also measured using the device specimen with several sensing electrode geometry, and a comparison was made between analysis and test. The effect of load resistance on the output voltage was then discussed experimentally, and the output power was evaluated.

2. ANALYSIS

2.1. Basic Equations

Equations of motion and Gauss' law are given by;

$$\sigma_{ji,j} = \rho u_{i,tt} \tag{1}$$

$$D_{i,i} = 0 \tag{2}$$

where σ_{ij}, u_i are the components of stress tensor and displacement vector, respectively, ρ is the mass density, D_i is the component of electric displacement vector, and a comma denotes partial differentiation with respect to the coordinates $x_i (i = 1, 2, 3)$ or the time *t*. We have employed Cartesian tensor notation and the summation convention over repeated tensor indices. Constitutive relations can be given by;

$$\varepsilon_{ij} = s_{ijkl}\sigma_{kl} + d_{kij}E_k \tag{3}$$

$$D_i = d_{ikl}\sigma_{kl} + \varepsilon_{ik}^T E_k \tag{4}$$

where ε_{ij}, E_i are the components of strain tensor and electric field intensity vector, respectively, and s_{ijkl}, d_{kij} and ε_{ik}^T are the elastic compliance, direct piezoelectric coefficient and permittivity at constant stress, which satisfy the following symmetry relations:

$$s_{ijkl} = s_{jikl} = s_{ijlk} = s_{klij}, d_{kij} = d_{kji}, \ \varepsilon_{ij}^T = \varepsilon_{ji}^T \tag{5}$$

*Address correspondence to this author at the Department of Materials Processing, Graduate School of Engineering, Tohoku University, Aoba-yama 6-6-02, Sendai 980-8579, Japan; Tel and Fax: +81-22-795-7342; E-mail: narita@material.tohoku.ac.jp

Table 1: Material Properties of BT

Elastic compliance					Direct piezoelectric coefficient			Permittivity		Mass density
(×10⁻¹² m²/N)					(×10⁻¹² m/V)			(×10⁻¹⁰ C/Vm)		(kg/m³)
s_{11}	s_{33}	s_{44}	s_{12}	s_{13}	d_{31}	d_{33}	d_{15}	ε_{11}^{T}	ε_{33}^{T}	ρ
8.85[a]	8.95[a]	22.8	-2.7	-2.9	-60[a]	140[a]	260	128	102[a]	5400[a]

[a] NEC/Tokin's product data sheets.

The train component is given by;

$$\varepsilon_{ij} = \frac{1}{2}(u_{j,i} + u_{i,j}) \tag{6}$$

and the component of electric field intensity vector is;

$$E_i = -\phi_{,i} \tag{7}$$

where ϕ is the electric potential. The constitutive relations (3) and (4) for piezoelectric ceramics poled in the x_3-direction are given in Appendix A.

2.2. Finite Element Method

Figure **1**(**a**) shows a composite cantilever constructed of BT and Cu layers under cyclic concentrated loads. Let the coordinate axes $x = x_1$ and $y = x_2$ be chosen such that they coincide with the interface and the $z = x_3$ axis is normal to this plane. The origin of the coordinate system is located at the center of the bottom left side of BT layer, and the edge at $x = 0$ is clamped. Figure **1**(**b**) shows the geometry and dimensions of the composite laminated cantilever with total thickness of 1.5 mm. BT layer (length l = 50 mm, width w = 25 mm, thickness 1 mm) is bonded to the upper surface of Cu layer (length 50 mm, width 25 mm, thickness 0.5 mm).

BT layer has sensing and driving electrodes, located at the center and outer parts of the top surface of the BT layer, respectively. The dimensions of the electrodes are shown in Figure **1**(**b**). The sensing electrode length is l_s, whereas the sensing electrode width is w_s. To suppress coupling, a grounding electrode is located between sensing and driving electrodes [10], and a whole grounding electrode is added on the opposite side.

ANSYS elements were defined by an eight-node 3D coupled field solid for the BT layer and an eight-node 3D structural solid for the Cu layer. For simplicity, the electrode layers were not considered in the finite element model. This is because the electrode layer thickness is much smaller than the BT layer thickness.

The left end (x = 0 plane) is clamped, and the laminated cantilever is under cyclic loads $P = (P_{max} + P_{min})/2 + \{(P_{max} - P_{min})\exp(i\omega t)\}/2$ at x = 49 mm, y = 0 mm and z = 1 mm, where P_{min} is a minimum load, P_{max} is a maximum load, and ω is an angular frequency. The top and bottom grounding electrode surfaces are connected to the ground, so that ϕ = 0. The electromechanical fields in the composite cantilever were then solved. Here, the statistical analysis was not carried out.

3. EXPERIMENTAL PROCEDURE

The composite cantilever was fabricated using BT ceramic layer (NEC/Tokin Co. Ltd., Japan) and Cu substrate. Electrodes were coated on both sides of the BT layer, and this BT layer with electrodes was bonded to the upper surface of the Cu layer using conductive bonding. Here, l_s = 10, 40 mm were considered. Table **1** lists the physical properties of the BT ceramics. Elastic compliances s_{11}, s_{33}, direct piezoelectric coefficients d_{31}, d_{33}, permittivity ε_{33}^T and mass density ρ can be found in the published data, while the remaining properties are assumed to be the same as those of BT ceramics reported in Ref. [11]. The elastic compliance, Poisson's ratio and mass density of Cu layer are 7.69×10^{-12} m²/N, 0.34 and 8920 kg/m³, respectively.

To generate cyclic loads P at the point (x = 49 mm, y = 0 mm, z = 1 mm) of the composite cantilever as illustrated in Figure **1**, a piezoelectric bimorph cantilever load cell was used. The lead wires were connected to the sensing and grounding electrodes, and output voltage V_{out} was measured using an oscilloscope. Various load resistances were applied. Then, the output power P_{out} from the harvester can be obtained by the output voltage V_{out} and load resistance R.

4. RESULTS AND DISCUSSION

Figure **2** shows the output voltage V_{out} versus maximum load P_{max} of the BT composite cantilevers with electrode length l_s = 10, 40 mm for minimum load
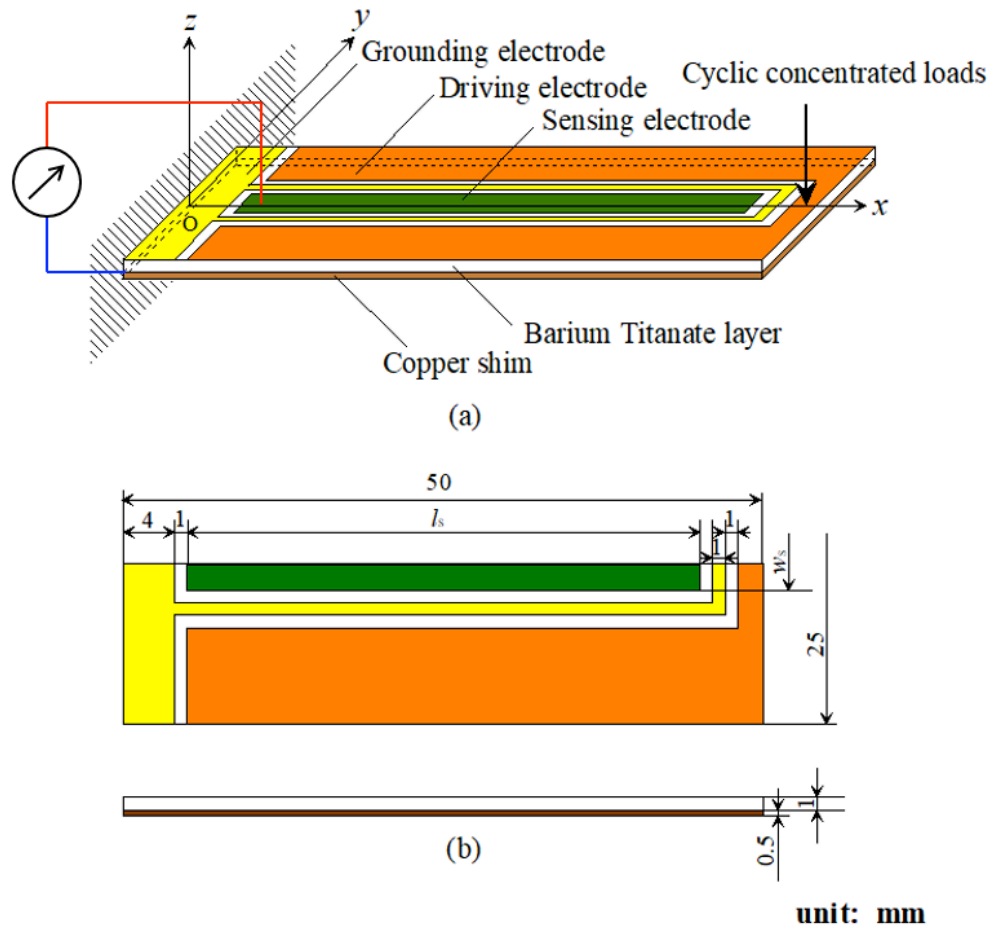
Figure 1: Schematic drawing of (**a**) BT laminated cantilever under concentrated load and (**b**) dimensions.

P_{min} = 0 N under frequency $f = \omega/2\pi$ = 50Hz at open circuit condition ($R \to \infty$). The lines and plots show the results of FEA and test, respectively. Reproducibility has been confirmed, hence one test result was shown. The results of FEA were in reasonable agreement with the test results. As is expected, the output voltage
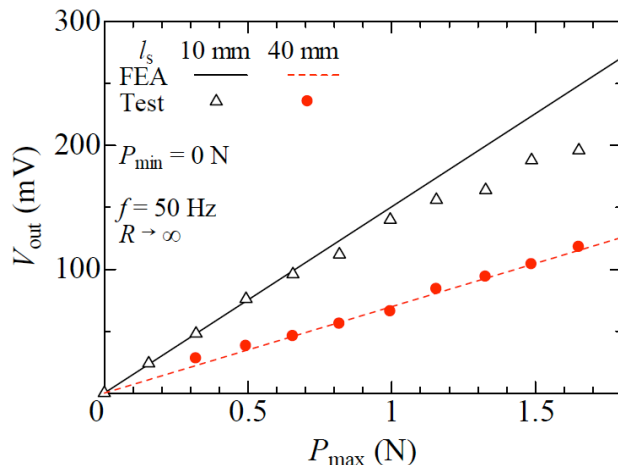
Figure 2: Output voltage versus maximum load of the BT laminated cantilevers.

increases when the maximum load increases. It is interesting to note that the output voltage of l_s = 10 mm is larger than that of l_s = 40 mm. Figure **3** shows the test results for the output voltage V_{out} versus frequency f of the BT composite cantilevers with l_s = 10, 40 mm for P_{max} = 2 N and P_{min} = 0 N at $R \to \infty$. When the frequency increases, the output voltage increases reaching a peak and then decreases. The output voltage of l_s = 10 mm is larger than that of l_s = 40 mm under all frequencies, and resonance frequencies are about 50 Hz. Figure **4** shows the test results for the output power P_{out} versus frequency f of the BT composite cantilevers with l_s = 10, 40 mm for P_{max} = 2 N and P_{min} = 0 N at R = 1 MΩ. The output power has some peak values. Similar to the output voltage, the output power of l_s = 10 mm is larger than that of l_s = 40 mm. Figure **5** shows the test results for the output power P_{out} versus load resistance R of the BT composite cantilever with l_s = 10 mm for P_{max} = 2 N and P_{min} = 0 N under f = 50 Hz. As the load resistance increases, the output power increases reaching a peak and then decreases. The peak value of the output power is observed at about R = 1.2 MΩ.
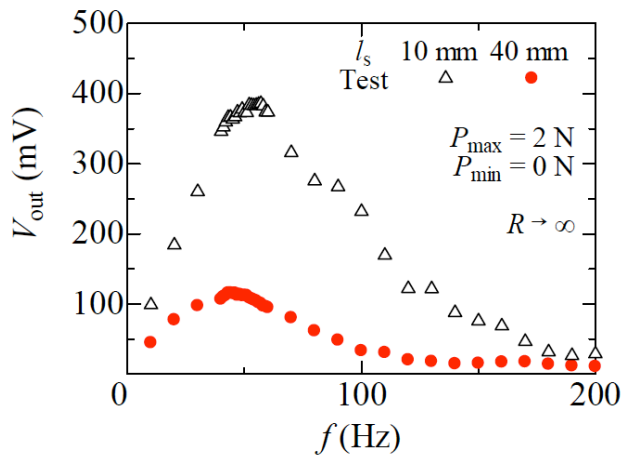
Figure 3: Output voltage versus frequency of the BT laminated cantilevers.
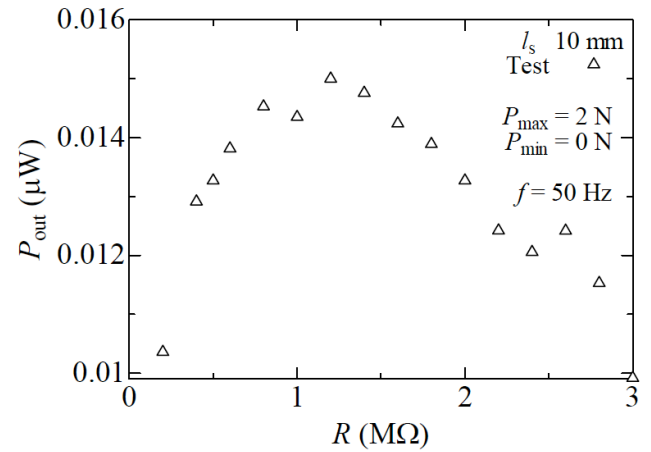
Figure 5: Output power versus load resistance of the BT laminated cantilever.
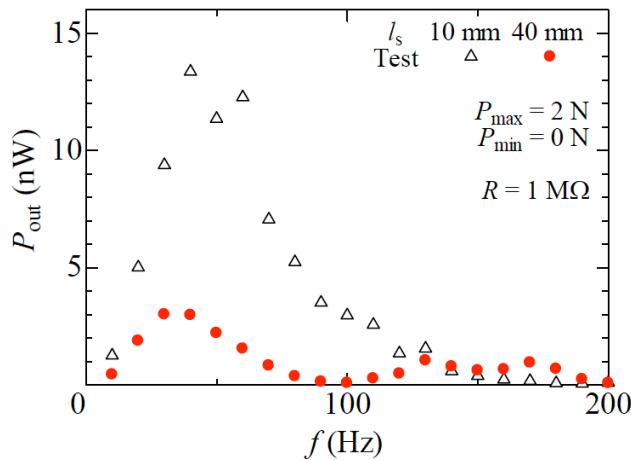
Figure 4: Output power versus frequency of the BT laminated cantilevers.
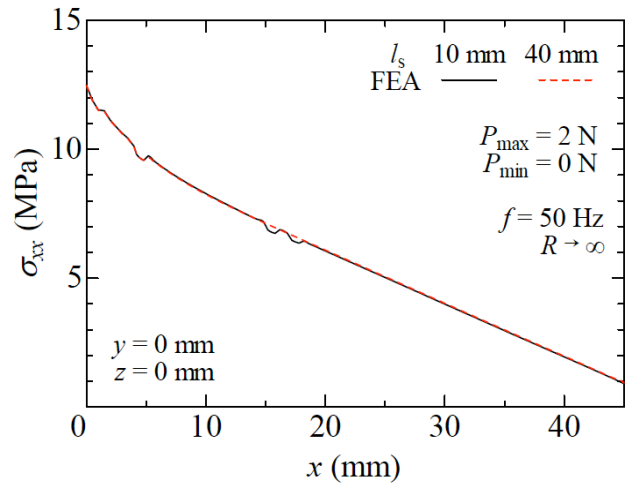
Figure 6: Normal stress distribution along the length direction of the BT laminated cantilevers.

Figure **6** shows the variations of normal stress σ_{xx} as a function of x at $y = 0$ mm and $z = 0$ mm of the BT composite cantilevers with $l_s = 10, 40$ mm for $P_{max} = 2$ N and $P_{min} = 0$ N at $R \rightarrow \infty$, obtained from the FEA. High normal stress is noted at the clamped end of the cantilevers. Note that the difference between the cantilevers with $l_s = 10, 40$ mm is very small.

CONCLUSION

A numerical and experimental investigation of the BT based composite laminated cantilevers under cyclic concentrated loads was conducted. On the basis of the study conducted, the following conclusions seem to be justified.

When the frequency increases, the output voltage and power increase, reaching a peak and then decrease.

The output voltage and power of the BT based composite laminated cantilever with small electrode are larger than those with large electrode.

High normal stress is noted at the clamped end, and the stress is independent of the sensing electrode geometry.

Appendix A

For piezoelectric ceramics which exhibit symmetry of a hexagonal crystal of class 6 mm with respect to principal x_1, x_2 and x_3 (poling) axes, the constitutive relations can be written in the following form:

$$
\begin{Bmatrix} \varepsilon_{11} \\ \varepsilon_{22} \\ \varepsilon_{33} \\ 2\varepsilon_{23} \\ 2\varepsilon_{31} \\ 2\varepsilon_{12} \end{Bmatrix} = \begin{bmatrix} s_{11} & s_{12} & s_{13} & 0 & 0 & 0 \\ s_{12} & s_{11} & s_{13} & 0 & 0 & 0 \\ s_{13} & s_{13} & s_{33} & 0 & 0 & 0 \\ 0 & 0 & 0 & s_{44} & 0 & 0 \\ 0 & 0 & 0 & 0 & s_{44} & 0 \\ 0 & 0 & 0 & 0 & 0 & s_{66} \end{bmatrix} \begin{Bmatrix} \sigma_{11} \\ \sigma_{22} \\ \sigma_{33} \\ \sigma_{23} \\ \sigma_{31} \\ \sigma_{12} \end{Bmatrix} + \begin{bmatrix} 0 & 0 & d_{31} \\ 0 & 0 & d_{31} \\ 0 & 0 & d_{33} \\ 0 & d_{15} & 0 \\ d_{15} & 0 & 0 \\ 0 & 0 & 0 \end{bmatrix} \begin{Bmatrix} E_1 \\ E_2 \\ E_3 \end{Bmatrix} \tag{A.1}
$$

$$
\begin{Bmatrix} D_1 \\ D_2 \\ D_3 \end{Bmatrix} = \begin{bmatrix} 0 & 0 & 0 & 0 & d_{15} & 0 \\ 0 & 0 & 0 & d_{15} & 0 & 0 \\ d_{31} & d_{31} & d_{33} & 0 & 0 & 0 \end{bmatrix} \begin{Bmatrix} \sigma_{11} \\ \sigma_{22} \\ \sigma_{33} \\ \sigma_{23} \\ \sigma_{31} \\ \sigma_{12} \end{Bmatrix} + \begin{bmatrix} \varepsilon_{11}^T & 0 & 0 \\ 0 & \varepsilon_{11}^T & 0 \\ 0 & 0 & \varepsilon_{11}^T \end{bmatrix} \begin{Bmatrix} E_1 \\ E_2 \\ E_3 \end{Bmatrix} \tag{A.2}
$$

Where;

$$
\sigma_{23} = \sigma_{32}, \qquad \sigma_{31} = \sigma_{13}, \qquad \sigma_{12} = \sigma_{21} \tag{A.3}
$$

$$
\varepsilon_{23} = \varepsilon_{32}, \qquad \varepsilon_{31} = \varepsilon_{13}, \qquad \varepsilon_{12} = \varepsilon_{21} \tag{A.4}
$$

$$
s_{11} = s_{1111} = s_{2222}, \qquad s_{12} = s_{1122}, \qquad s_{13} = s_{1133} = s_{2233}, \qquad s_{33} = s_{3333},
$$
$$
s_{44} = 4s_{2323} = 4s_{3131}, \qquad s_{66} = 4s_{1212} = 2(s_{11} - s_{12}) \tag{A.5}
$$

$$
d_{15} = 2d_{131} = 2d_{223}, \qquad d_{31} = d_{311} = d_{322}, \qquad d_{33} = d_{333} \tag{A.6}
$$

REFERENCES

[1] Shindo Y and Narita F. Dynamic bending/torsion and output power of S-shaped piezoelectric energy harvesters. International Journal of Mechanics and Materials in Design 2014; 10: 305-311.
https://doi.org/10.1007/s10999-014-9247-0

[2] Mori K, Shindo Y, Narita F and Okura S. Detection and response characteristics of giant magnetostrictive / piezoelectric laminated cantilevers under cyclic bending. Mechanics of Advanced Materials and Structures, in press.
https://doi.org/10.1080/15376494.2014.949924

[3] Vatansever D, Hadimani RL, Shah T and Siores E. An investigation of energy harvesting from renewable sources with PVDF and PZT, Smart Materials and Structures 2011; 20: 055019.
https://doi.org/10.1088/0964-1726/20/5/055019

[4] Wong VK, Ho JH and Yap EH. Dynamics of a piezoelectric beam subjected to water droplet impact with water layer formed on the surface, Journal of Intelligent Material Systems and Structures, in press.
https://doi.org/10.1177/1045389X14549871

[5] Okayasu M and Watanabe K. The electric power generation characteristics of a lead zirconate titanate piezoelectric ceramic under various cyclic loading conditions, Ceramics International (2015).
https://doi.org/10.1016/j.ceramint.2015.08.076

[6] Wang Y and Inman DJ. Simultaneous energy harvesting and gust alleviation for a multifunctional composite wing spar using reduced energy control *Via* piezoceramics. Journal of Composite Materials 2013; 47-1: 125-146.

[7] Narita F and Shindo Y. Piezoelectric detection and response characteristics of barium titanate unimorph cantilevers under AC electric fields. International Journal of Metallurgical and Materials Engineering, in press.
https://doi.org/10.15344/2455-2372/2015/103

[8] Cohen RE. Origin of ferroelectricity in perovskite oxides. Nature 1992; 358: 136- 138.
https://doi.org/10.1038/358136a0

[9] Saito Y, Takao H, Tani T, Nonoyama T, Takatori K, *et al*. Lead free piezoceramics, Nature 2004; 432: 84-87.
https://doi.org/10.1038/nature03028

[10] Wakatsuki N, Yokoyama H and Kudo S. Piezoelectric actuator of LiNbO3 with an integrated displacement sensor Jpn. J Appl Phys 1998; 37: 2970-2973.
https://doi.org/10.1143/JJAP.37.2970

[11] Jaffe H and Berlin court DA. Piezoelectric transducer material, Proceedings IEEE 1965; 53: 1372.
https://doi.org/10.1109/PROC.1965.4253